Title

Preventive Treatment with a CD73 Small Molecule Inhibitor Enhances Immune Surveillance in K-Ras Mutant Pancreatic Intraepithelial Neoplasia.

Journal

Cancer Prevention Research, 17(10)

Authors

Strickland, Lincoln

Liu, Wendao

Hussein, Usama

et al.

Publication Date

2024-10-01

DOI

10.1158/1940-6207.CAPR-24-0200

Peer reviewed

Preventive Treatment with a CD73 Small Molecule Inhibitor Enhances Immune Surveillance in K-Ras Mutant Pancreatic Intraepithelial Neoplasia

Lincoln N. Strickland[1], Wendao Liu[2,3], Usama Hussein[3,4], Nicolette Mardik[1], Xian Chen[3], Tingting Mills[5], Lana A. Vornik[6], Michelle I. Savage[6], Shizuko Sei[7], John Clifford[7], Holger K. Eltzschig[1], Powel H. Brown[6], Zhongming Zhao[3], Florencia McAllister[6,8,9], and Jennifer M. Bailey-Lundberg[1,2,10]

ABSTRACT

Immunoprevention is an emerging consideration for solid tumors, including pancreatic ductal adenocarcinoma (PDAC). We and others have shown that Kras mutations in genetic models of spontaneous pancreatic intraepithelial neoplasia (PanIN), which is a precursor to PDAC, results in CD73 expression in the neoplastic epithelium and some populations of infiltrating immune cells, including macrophages and CD8 T cells. CD73 is an ecto-enzyme that converts extracellular adenosine monophosphate to adenosine, a critical immune inhibitory molecule in PDAC. We hypothesized inhibition of CD73 would reduce the incidence of PanIN formation and alter the immune microenvironment. To test our hypothesis, we used the *Kras*^{G12D}; *Pdx*^{Cre1} (*KC*) genetically engineered mouse model and tested the utility of AB-680, a small molecule inhibitor targeting CD73, to inhibit PanIN progression. AB-680, or vehicle control, was administered using oral gavage delivery 3 days/week at 10 mg/kg, beginning when the mice were 2 months old and lasting 3 months. We euthanized the mice at 5 months old. In the *KC* model, we quantified significantly less pancreatitis, early and advanced PanIN, and quantified a significant increase in M1 macrophages in AB-680-treated mice. Single-cell RNA sequencing (scRNA-seq) of pancreata of AB-680-treated mice revealed increased infiltration of CD4$^+$ T cells, CD8$^+$ T cells, and mature B cells. The scRNA-seq analysis showed that CD73 inhibition reduced M2 macrophages, acinar, and PanIN cell populations. CD73 inhibition enhanced immune surveillance and expanded unique clonotypes of TCR and BCR, indicating that inhibition of CD73 augments adaptive immunity early in the neoplastic microenvironment.

Prevention Relevance: Previous studies found PanIN lesions in healthy pancreata. Not all progress to PDAC, suggesting a window for enhanced antitumor immunity through immunoprevention therapy. CD73 inhibition in our study prevents PanIN progression, reduces immunesuppressive macrophages and expands TCR and BCR unique clonotypes, highlighting an encouraging therapeutic avenue for high-risk individuals.

Introduction

Immunoprevention, an emerging approach to improve antitumor immune surveillance, is being considered for solid tumors such as pancreatic ductal adenocarcinoma (PDAC). Pancreatic intraepithelial neoplasia (PanIN) is a precursor to PDAC, and mutations in *KRAS* are common in PanIN. As shown previously, PanIN lesions are present in most adult healthy human pancreas tissue (1, 2). However, most PanINs have not progressed to PDAC, indicating a window of opportunity to utilize immunoprevention therapies to enhance

[1]Department of Anesthesiology, Critical Care and Pain Medicine, McGovern Medical School, The University of Texas Health Science Center at Houston, Houston, Texas. [2]The University of Texas MD Anderson Cancer Center UTHealth Houston Graduate School of Biomedical Sciences, Houston, Texas. [3]Center for Precision Health, McWilliams School of Biomedical Informatics, The University of Texas Health Science Center at Houston, Houston, Texas. [4]Department of Lymphoma and Myeloma, The University of Texas MD Anderson Cancer Center, Houston, Texas. [5]Department of Biochemistry, McGovern Medical School, The University of Texas Health Science Center at Houston, Houston, Texas. [6]Department of Clinical Cancer Prevention, The University of Texas MD Anderson Cancer Center, Houston, Texas. [7]Division of Cancer Prevention, National Cancer Institute, Rockville, Maryland. [8]Department of Gastrointestinal Medical Oncology, The University of Texas MD Anderson Cancer Center, Houston, Texas. [9]Department of Immunology, The University of Texas MD Anderson Cancer Center, Houston, Texas. [10]Department of Pathology, Microbiology and Immunology, The University of Nebraska Medical Center, Omaha, Nebraska.

L.N. Strickland, and W. Liu contributed equally to this article.

Corresponding Author: Jennifer M. Bailey-Lundberg, Department of Pathology, Microbiology and Immunology, The University of Nebraska Medical Center, Fred and Pamela Buffett Cancer Center, 4.12.400, Omaha, NE 68198. E-mail: jlundberg@unmc.edu

Cancer Prev Res 2024;17:457–70

doi: 10.1158/1940-6207.CAPR-24-0200

antitumor immune surveillance and prevent the progression of early precancerous PanIN lesions from developing into PDAC. CD73, an ectonucleotidase enzyme that generates extracellular adenosine, is not expressed in normal physiologic pancreatic acinar cells and is expressed at low levels in pancreatic ducts. However, we and others have detected CD73 in a subset of premalignant epithelial lesions such as PanIN and intrapapillary mucinous neoplasia (IPMN; refs. 3, 4). Elevated CD73 in these lesions indicates that CD73-generated adenosine may be a critical signaling mechanism orchestrating immune suppression in the PanIN microenvironment (5, 6). Our group has previously shown treatment with CD73 inhibitors reduces the spontaneous development of PDAC in genetically engineered mouse (GEM) models with high expression of CD73 and elevated intratumoral adenosine concentrations (4), leading us to explore the use of CD73 inhibitors to prevent the progression of Kras-mutant PanIN.

CD73-generated adenosine and subsequent adenosine signaling mechanisms are utilized by cells to reduce inflammation in proinflammatory and hypoxic environments (7, 8). Extracellular ATP and ADP can be converted to AMP by an ectonucleotidase enzyme (CD39), and AMP is then converted to adenosine by CD73. In the tumor microenvironment (TME), extracellular adenosine can also be released by stressed or injured cells (9) and signals through one of four GPCR adenosine receptors (A_1R, $A_{2A}R$, $A_{2B}R$, and A_3R), which are co-expressed on epithelial, stromal, tumoral, and immune cells (10).

Macrophages, a type of white blood cell and essential arm of the innate immune system, have long been studied in the context of response to foreign pathogens and are known for various functions, including engulfment and digestion of microorganisms. Macrophages are also critical in the removal and clearance of dead cells and residual debris and can stimulate a more robust immune response. Integral to these functions, macrophages are polarized into many different subtypes. Classically activated macrophages (M1) are proinflammatory antigen-presenting cells and can release inflammatory cytokines (11). Alternatively activated macrophages (M2) are anti-inflammatory or immune suppressive, increase fibrosis, and promote angiogenesis (12).

In PDAC, macrophages are one of the earliest immune cells to infiltrate the neoplastic and tumor microenvironment, and several preclinical studies have demonstrated macrophages in PDAC contribute to immune suppression, desmoplasia, resistance to therapeutics, angiogenesis, and stem cell features of cancer cells (13). Therapeutic approaches to reduce the immune suppressive functions of alternatively activated macrophages are encouraged to improve responses to chemotherapy and immunotherapies. Our study suggests inhibiting CD73 reduces M2 polarization, and through Gene Ontology (GO) analysis of single-cell RNA sequencing (scRNA-seq) data, we show inhibition of CD73 elevates pathways related to cytoplasmic translation and RNA splicing. Our scRNA-seq data also indicates inhibiting CD73 boosts intrapancreatic CD4 and CD8 T-cell expansion and promotes increased clonogenicity of T-cell receptors (TCR). Increased TCR clonogenicity improves responses to immunotherapy and, when expanded in pancreatic tumors, is correlated with better overall survival (14). Thus, our data show inhibiting CD73 has more critical effects on CD4 and CD8 T cells than previously demonstrated.

Materials and Methods

Mouse models

All mouse models and procedures comply with animal welfare guidelines. We used the genetically engineered $Kras^{G12D}/Pdx^{Cre1}$(*KC*) mouse model, which slowly developed PanIN and PDAC over 12 to 15 months. Mice were enrolled in the study after genotyping by tail PCR. At the experimental endpoint, mice were euthanized by isoflurane overdose, and blood, serum, and pancreas tissue were collected. For this study, $n = 8$ vehicle control animals and $n = 11$ AB-680-treated animals. All animal experiments were conducted in accordance with ARRIVE guidelines and were approved by the University of Texas Health Science Center IACUC Committee. Sex as a biological variable: both male and female mice were used in the experiment.

CD73 inhibitor administration

AB-680 (HY-125286) was dissolved in 20% SBE-β-CD (MedChem Express, HY-17031/CS-0731) and DMSO (Sigma-Aldrich, D8418) and administered oral gavage 10 mg/kg 3 days a week. The vehicle control was DMSO in 20% SBE-β-CD and administered oral gavage 3 days a week.

Immunohistochemistry and ImageJ analysis

Tissues were fixed in zinc-buffered formalin, processed, and embedded in paraffin. Sections were placed on positively charged slides and baked at 60°C for 30 minutes. Slides were deparaffinized in histoclear and gradually rehydrated to PBS. Heat-mediated antigen retrieval was performed using a microwave-based method, a pH 6 solution (Vector Laboratories, H-3300), or a pH 9 solution (Abcam 100× Tris-EDTA, ab 93684). Sections were blocked for 1 hour at room temperature (RT) in 10% FBS in PBST. Primary antibodies were diluted in a blocking solution and incubated overnight at 4°C. Primary antibodies used and the accompanying dilutions are listed as follows: CD73 (1:200, D7F9A), Cytokeratin-19 (1:150, ab52625), Granzyme B (1:200, ab255598), Ki-67 (1:200, ab15580), Myeloperoxidase (1:200, ab208670), NIMPR-14 (1:100, ab2557), CD68 (1:100, ab283654), CD163 (1:500, ab182422), iNOS (1:100, ab15323), B3GAT1 (1:200, PA-5-86578). Tissues were washed three times with PBS for 5 minutes and incubated in secondary antibody (Vector Laboratories, BA-1000, BA-9400) at RT for 30 minutes at a 1:500 dilution in blocking buffer. Tissues were washed three times with PBS for 5 minutes and incubated using the Vectastain ABC kit Peroxidase Standard (Vector Laboratories, PK4000). Tissues

were washed three times with PBS for 5 minutes, then the DAB peroxidase (HRP) Substrate kit (Vector Laboratories, SK-4100) was used. Tissues were rinsed in tap water for two changes of 5 minutes and were stained in hematoxylin, then gradually dehydrated in ethanol. Tissues were cleared in histoclear and mounted. Analysis of immunohistochemistry images was performed using ImageJ software (https://imagej.net; Supplementary Fig. S1A–S1F). Five to ten representative fields per tissue were used depending on tissue size. A freehand selection tool was used to determine pancreatitis, PanIN, and PDAC area. The color threshold tool was used to determine positive staining in each field.

Alcian blue

Tissues were fixed in zinc-buffered formalin, processed, and embedded in paraffin. Slides were deparaffinized in histoclear and rehydrated in distilled water. Slides were incubated in Acetic Acid solution for 3 minutes at room temperature (RT). Slides were incubated in Alcian Blue solution for 45 minutes at RT. Slides were rinsed for 1 minute with tap water, followed by a 10-second wash in distilled water. Slides were stained in Safranin O solution for 5 minutes. Slides were rinsed for 1 minute with tap water, followed by a 10-second wash in distilled water. Tissues were dehydrated through graded alcohols, cleared in histoclear, and mounted.

Trichrome

Tissues were stained according to the recommended protocol of the trichrome staining kit (ab150686). Tissues were deparaffinized for 9 minutes in histoclear and hydrated gradually in ethanol to distilled water. Slides were placed in preheated Bouin's fluid for 60 minutes and rinsed in running tap water until sections were clear. Slides were placed in tap water for 4 minutes and stained with working Weigert's iron hematoxylin for 5 minutes. Slides were rinsed for 2 minutes in running tap water and then stained with biebrich scarlet/acid fuchsin solution for 15 minutes. Slides were rinsed in distilled water and stained with phosphomolybdic/phosphotungstic acid solution for 10 minutes. Without rinsing, slides were stained with aniline blue solution for 10 minutes. Slides were rinsed in distilled water and placed in acetic acid solution for 5 minutes. Then, the slides were dehydrated in 95% ethanol and 100% ethanol, then mounted.

Hematoxylin and eosin

Tissues were placed in histoclear for 8 minutes, 100% ethanol for 4 minutes, and 95% for 2 minutes. Tissues were put in the following order for 3 minutes each: tap water, hematoxylin, and tap water. Next, tissues were left in the following order for 1 minute each: clarifier, tap water, bluing agent, water, 95% ethanol, eosin, and 95% ethanol. Tissues were placed for 4 minutes in 100% ethanol and 4 minutes in histoclear, then mounted.

Nucleoside purification and high-performance liquid chromatography

Methods described previously (15).

Sample acquisition and tissue processing for scRNA-seq

Pancreas tissue from two mice per group was collected. After processing, the two tissues from each respective group were combined and submitted as one sample per group to the Cancer Genomics Center at UTHealth. After collection, the tissue was placed in ice-cold PBS, then minced thoroughly on a glass surface on ice for about 2 minutes until it was a fine paste. Tissue was added to 1 mL type 4 collagenase enzyme mix (50 μL type 4 collagenase 100 mg/mL, 5 μL DNAse, 10 μL RNAse inhibitor, 5 μL 1 mol/L $CaCl_2$, 10 μL 10% BSA/PBS, 930 μL DPBS). Samples were incubated on ice and shaken gently every 30 seconds for 2 minutes. Then we triturated 10 times per minute for 20 minutes. Chunks were allowed to settle over ice for 1 minute. A total of 750 μL of supernatant containing whole cells were filtered on a 30 μmol/L filter over a 50 mL conical tube. The filter was rinsed with 5 mL ice-cold PBS/BSA 0.04%. To the remaining tissue chunks, 1 mL type 4 collagenase enzyme mix was added and triturated on ice 10 times every minute for 30 minutes. The entire volume of the sample was added onto the same filter over the 50 mL conical and rinsed with 5 mL ice-cold PBS/BSA 0.04%. Flow through was transferred to 15 mL conical and centrifuged at 300 *g* for 5 minutes at 4°C. The supernatant was removed, and the pellet was resuspended in 100 μL ice-cold PBS/BSA 0.04%. A total of 10 mL ice-cold PBS/BSA 0.04% was added, and the sample was centrifuged for 5 minutes at 300 *g* at 4°C. The supernatant was removed, and the pellet was resuspended in 100 μL ice-cold PBS/BSA 0.04%. The single cells were filtered using a 40-μm cell strainer and examined under a microscope to confirm successful dissociation into individual cells before sequencing.

scRNA library and TCR/BCR V(D)J repertoire library preparation

The Cancer Genomics Core at UTHealth processed single-cell suspensions and prepared libraries for 10× Genomics following the manufacturer's guidelines. The single cell capture and library construction were performed by following the Chromium Next GEM Single cell 5′ Reagent Kits v2 protocol (CG000331). Briefly, cells were resuspended in PBS with 0.04% BSA at a concentration of 700 to 1,200 cells/μL and more than 85% viability. The single cells were loaded onto Chromium Next GEM Chip K with partitioning oil and barcoded single-cell gel beads. Approximately 3,000 cells per sample were captured. The barcoded and full-length cDNA is produced after the gel beads-in-emulsion (GEM) incubation and amplified via PCR for library construction. The library preparation is performed by following the protocol of Chromium Next GEM Single Cell 5′ GEM, Library & Gel Bead Kit v2 (PN-1000267). The RNA and TCR/BCR libraries

were generated from the same cells with identical cell barcodes. The quality of the final libraries was examined using an Agilent High Sensitive DNA Kit (#5067-4626) on an Agilent Bioanalyzer 2100 (Agilent Technologies). The qualified libraries were used for paired-end sequencing on an Illumina NovaSeq System (Illumina, Inc.).

scRNA-seq data analysis

We processed the raw data from paired scRNA library, single-cell TCR library, and single-cell BCR library using Cell Ranger (v7.0.0) multi pipeline. The RNA library was aligned to mm10-2020-A reference genome, and the TCR and BCR libraries were aligned to GRCm38-alts-ensembl-7.0.0 provided by 10× Genomics. The output files from Cell Ranger included UMI count matrix generated from RNA library and assembled contigs with annotations generated from TCR and BCR libraries. As we detected ambient RNA contamination from acinar and PanIN cells, we used CellBender (v3.0.0) to correct the raw UMI count matrix from Cell Ranger output (16). The corrected UMI count matrix output_filtered.h5 from CellBender were used for analysis. Subsequently, detailed QC metrics were computed and assessed using Seurat package (v4.1.1; ref. 17). Cells with less than 200 genes, more than 7,000 genes or more than 15% mitochondrial gene counts were filtered to ensure data quality. The filtered data were then normalized by library size and $\log_2$-transformed. We further removed inferred doublets using scDBlFinder (v.1.8.0; ref. 18) and erythrocytes. Subsequently, 3,000 highly variable genes were selected for dimension reduction and clustering analysis. To assess for batch effects, results from principal component analysis (PCA), 2D uniform manifold approximation and projection (UMAP) dimension reduction plots, and sample-by-cluster distributions were carefully reviewed. Integrated information revealed minimal batch effects. We used *FindNeighbors* function with first 25 PCs and parameter $K = 10$ to build the nearest neighbor graph and then used *FindClusters* function with the resolution 1.5 to identify single-cell clusters. The UMAP method was employed for dimensionality reduction and 2D visualization of the single-cell clusters. Differential expression analysis was performed using the Wilcoxon ranked-sum method. We annotated cell types by examining the expression of canonical cell markers in cell clusters. The difference in cell proportion between two conditions of a cell type was tested using Fisher exact test.

Single-cell TCR/BCR sequencing data analysis

We used the filtered_contig_annotations.csv file from Cell Ranger output and scRepertiore (19) to analyze TCR and BCR clonotypes. For TCRs, we found that the alpha-chain (TRA) of many single cells was not captured in library preparation and sequencing, so we defined TCR clonotypes based on beta-chain (TRB) complementarity-determining region 3 (CDR3) amino acid sequence. For BCRs, we defined clonotypes based on both heavy-chain (IGH) and light-chain (IGL) CDR3 amino acid sequence. We added the immune repertoire information to T-cell and B-cell subpopulations using function *combineExpression*. TCR/BCR clonotypes were grouped according to the clone size to measure the clonal expansion. We compared the TCR/BCR clonotypes in two experimental conditions and multiple T- or B-cell subpopulations. Lineage tracing of TCR/BCR was conducted by considering all clonotypes shared by cells from more than one cell subpopulations. We measured the overlap of clonotypes using overlap coefficient, calculated from the intersection of two sets of clonotypes divided by the size of the smaller set.

GO enrichment analysis

The GO is a widely utilized biological database. To analyze the differentially expressed genes between AB-680 treatment and vehicle control in each cell type, we used the *enrichGO* function from the clusterProfiler package to find the enriched GO biological processes terms (20). The differentially expressed genes were calculated using the *FindMarkers* function. We used the upregulated genes in each cell type to identify significantly enriched terms and pathways in AB-680 treatment.

Data availability

All the raw and processed data supporting the findings of this study are available through GEO, accession number GSE273209. The R and Python scripts supporting the findings of this paper are available upon request.

Results

AB-680 treatment suppresses PanIN progression in KrasLSL-G12D; Pdx-1Cre (*KC*) mice

To evaluate the efficacy of AB-680 for the progression of PanIN *in vivo*, we used the $Kras^{G12D}/Pdx^{Cre1}$ (*KC*) mouse model (**Fig. 1A**). *KC* mice develop the entire spectrum of PanIN lesions and eventually develop PDAC; therefore, they are an ideal model for a preclinical study on prevention (21). Immunohistochemical (IHC) staining showed CD73 expression in a subset of early PanIN in these mice (**Fig. 1B**). Therefore, we treated *KC* mice through oral gavage delivery with either 10 mg/kg AB-680 or a 10 mg/kg SBE-DMSO vehicle control 3 days a week. We began treatment when the mice were 2 months old and continued therapy for 3 months until the experimental endpoint when the mice reached 5 months old. Pancreas tissue was harvested and used for IHC analysis, scRNA-seq, and high-performance liquid chromatography (HPLC; **Fig. 1C**). Upon histological examination of a hematoxylin and eosin (H&E) staining, we quantified a significant decrease in the incidence of pancreatitis ($P < 0.05$; **Fig. 1D**; Supplementary Fig. S1G). We also quantified a significant decrease in early PanIN lesions ($P < 0.0001$), defined as epithelial lesions comprised of mucin-containing columnar cells with basally located nuclei (22, 23). We also determined a significant decrease in advanced PanIN lesions ($P < 0.05$; **Fig. 1E**; Supplementary Fig. S1H

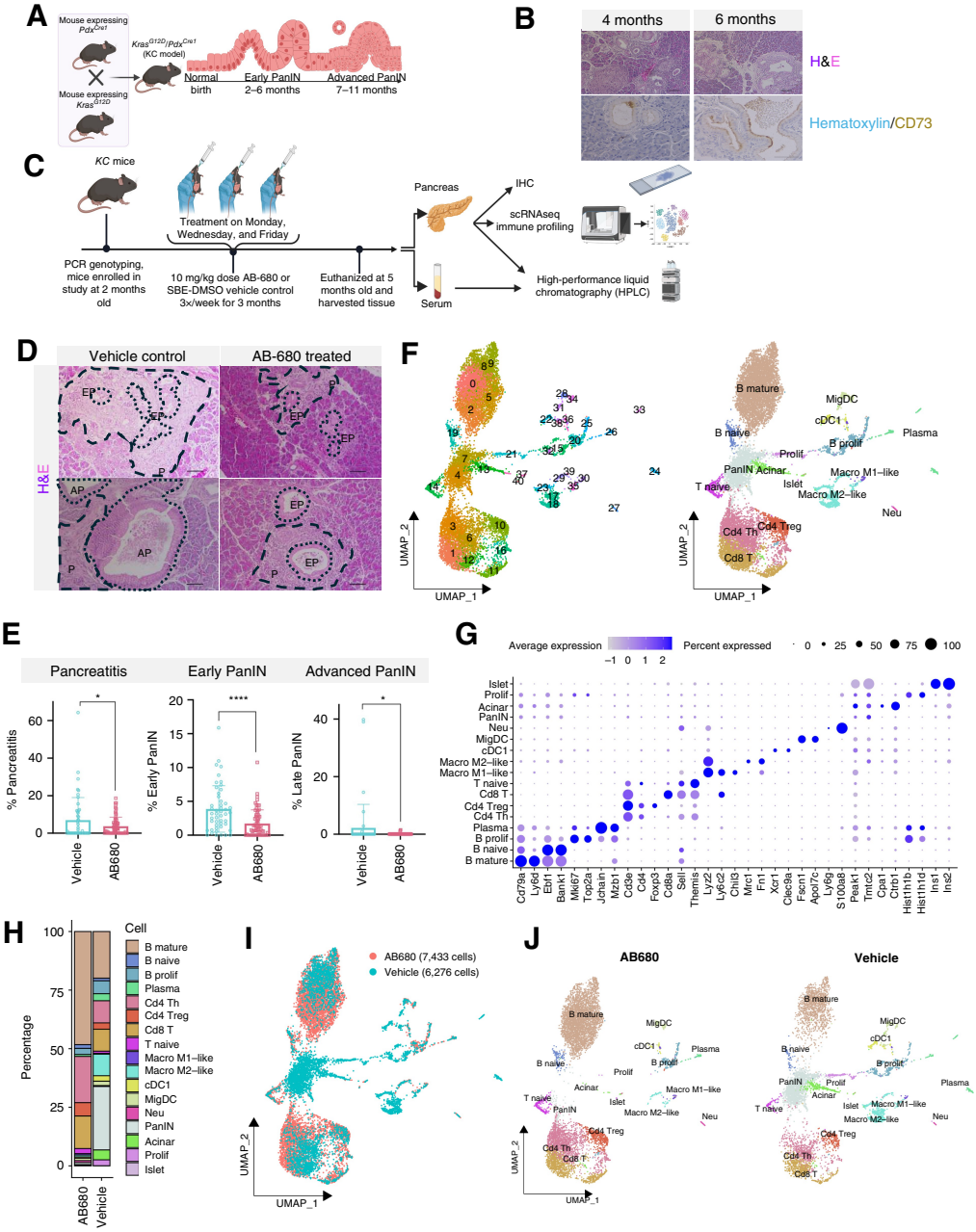

Figure 1.

Treatment with the CD73 small molecule inhibitor AB-680 significantly reduces early to advanced PanIN progression in *KC* mice, and scRNA-seq reveals cell-type composition in the pancreas of 5-month-old *KC* mice. **A,** Schematic of *Kras*^{G12D}/*Pdx*^{Cre1} (*KC* model) breeding scheme and timeline of PanIN development. **B,** Representative H&E 20× images of the *KC* model at different timepoints. Representative 40× images CD73 staining of the *KC* model at different timepoints. **C,** Schematic of experimental flow for *KC* model. Mice are genotyped through tail DNA PCR and enrolled into the study at 2 months old. Treatment begins immediately and either a vehicle control or AB-680 is given 3×/week at a 10 mg/kg dose. Treatment continues for between 3 months until the mice are humanely euthanized at 5 months old. Serum is collected and used for HPLC analysis. Pancreas tissue is harvested and used for IHC, scRNA-seq immune profiling, and HPLC. **D,** H&E staining 20× images of pancreatitis, early PanIN, and advanced PanIN in vehicle control and AB-680 pancreas tissue. Pancreatitis (P) areas are outlined with the dashed line, and early PanIN (EP) and advanced PanIN (AP) are outlined with the dotted line. **E,** AB-680 treatment significantly decreases pancreatitis incidence (*, $P = 0.0481$). AB-680 treatment significantly decreases early PanIN (****, $P < 0.0001$). AB-680 treatment significantly decreases advanced PanIN (*, $P = 0.0372$). All quantification was performed in ImageJ, $n = 8$ vehicle control, $n = 11$ AB-680, and six fields per mouse were analyzed. Statistical analysis was performed using a Student *t* test in Prism GraphPad software. Scale bars, 100 μm. **F,** UMAP visualization displaying cell clusters and annotated cell types in AB-680-treated group and vehicle control group in the scRNA-seq data. **G,** Dot plot illustrating the expression of marker genes across different cell populations. **H,** Comparison of cell population frequencies in scRNA-seq data between the two experimental conditions. **I,** UMAP visualization highlighting the cells in AB-680-treated group and vehicle control group. **J,** UMAP projections depicting the segregation of cell types between the AB-680-treated and vehicle control groups. (**E,** Created with BioRender.com.)

and S1I) in the AB-680-treated mice compared to vehicle control–treated mice, defined as larger, frequently stratified papillary lesions with a loss of nuclear polarity and budding off small clusters of epithelial cells (22, 23).

scRNA-seq reveals cell-type composition in the pancreas of 5-month-old *KC* mice

To comprehensively assess the impact of CD73 small molecule inhibitor on the PanIN microenvironment, we utilized simultaneous scRNA, TCR, and BCR sequencing (scRNA/TCR/BCR-seq) to analyze dissociated whole pancreata from mice treated with either vehicle or AB-680, isolated at the time of euthanasia. The scRNA-seq analysis revealed 17 distinct cell types, including mature B cells, naive B cells, proliferative B cells, plasma cells, $CD4^+$ helper T (Th) cells, $CD4^+$ regulatory T (Treg) cells, $CD8^+$ T cells, naïve T cells, M1-like macrophages, M2-like macrophages, conventional dendritic cells 1 (cDC1), migratory dendritic cells (MigDC), neutrophils, PanIN cells, acinar cells, proliferative PanIN cells, and islet cells annotated from 41 clusters (**Fig. 1F**). We used canonical and previously reported cell markers to annotate these cell types. B cells were identified with high *Cd79a*, *Ly6d*, and *Ms4a1 expression*. Naive B cells had high expression of *Ebf1* and *Bank1*. Proliferative B cells had high expression of Mki67 and *Top2a*. Plasma cells had high expression of *Jchain* and *Mzb1*. T cells were identified with high expression of *Cd3e* and further divided by the expression of *Cd4* and *Cd8a*. Regulatory T cells were identified with high expression of *Foxp3*. Naive T cells were identified with high expression of *Themis* and *Sell* (24). Macrophages were identified with high expression of Lyz2. The pro-inflammatory M1-like macrophages had high expression of *Ly6c2* and *Chil3* (25), while M2-like macrophages had high expression of *Mrc1* and *Fn1* (26). cDC1 were identified with high expression of *Xcr1* and *Clec9a* (27). MigDC were identified with high expression of *Fscn1* and *Apol7c* (27). Neutrophils were identified with high expression of *Ly6g* and *S100a8*. PanIN cells were identified with high expression of *Peak1* and *Tmtc2* (28). A proliferative cell cluster was found with high expression of *Hist1h1b* and *Hist1h1d*, mainly comprising proliferative PanIN cells. Acinar cells were identified with high expression of *Cpa1* and *Ctrb1* (29). Islet cells were identified with high expression of *Ins1* and *Ins2*. The dot plot illustrated the average expression level and the expressed cell percentage of specific marker genes in each cell type (**Fig. 1G**). In addition, the proportion of cell types distributed between AB-680-treated and vehicle control groups (**Fig. 1H**) showed T- and B-cell populations are more expanded in AB-680-treated group versus vehicle control. A Heat map displaying the top 10 genes in each cell type, along with feature plots for the specific features used for cell type identification, is provided in Supplementary Fig. S2A and S2B; Supplementary Table S1.

The UMAP projection of cells treated with AB-680 (red) and the vehicle control (blue) revealed a clear distribution difference between the AB-680-treated and control groups. The AB-680-treated group showed a higher cell proportion than the control group (**Fig. 1I** and **J**). The UMAP embedding between the two conditions showed an apparent effect of AB-680 on the PanIN, proliferative PanIN, acinar cells, and M2-like macrophages, with AB-680 treatment resulting in a reduced abundance of these cell types (**Fig. 1I** and **J**). This suggests that AB-680 treatment had a potent suppressive effect on both PanIN and tumor-associated macrophages.

CD73 inhibition reduces $CK19^+$ neoplasia, fibrosis, and proliferation in dysplastic lesions in *KC* mice

To assess inflammation, proliferation, and fibrosis, we performed additional staining in the pancreata of the experimental *KC* mice treated with AB-680 or the vehicle. We stained for cytokeratin-19 (CK-19) and found a significant decrease in CK-19 staining in the AB-680 treated mice ($P < 0.0001$; **Fig. 2A** and **B**). scRNA-seq data also confirmed a significant reduction in the proportion of PanIN ($P < 0.0001$) and proliferative PanIN cells ($P < 0.0001$) in response to AB-680. (**Fig. 2C**). We also stained for Alcian Blue (mucin expression), Ki-67 and performed a Trichrome stain, and quantified a significant decrease in mucin expression ($P < 0.0001$), Ki-67 ($P < 0.0001$), and Trichrome collagen abundance ($P < 0.0001$) in the AB-680 treated mice compared to the vehicle-treated mice (**Fig. 2A** and **B**). These data are also confirmed by decreased expression of *Mki67* in proliferative PanIN from the scRNA-seq analysis (**Fig. 2D**).

CD73 promotes M2 macrophage polarization in the PanIN microenvironment

Neutrophils and macrophages are highly abundant in PDAC and are essential for orchestrating immune suppression in the PDAC TME (30). To assess neutrophil and macrophage abundance in the pancreata of *KC* AB-680-treated and vehicle-treated mice, we performed IHC staining. We stained for Myeloperoxidase (MPO), a heme-containing peroxidase expressed by neutrophils, monocytes, and macrophages. We found a significant increase in MPO staining in AB-680-treated mice compared to vehicle-treated mice ($P < 0.001$; **Fig. 2E** and **F**). To examine neutrophil populations, we stained for NIMPR-14 and did not quantify a significant difference in neutrophil abundance between groups (Supplementary Fig. S3A and S3B). We also assessed cytotoxic immune cells by staining for Granzyme B and dendritic cells by B3GAT1 and found no significant difference between groups (Supplementary Fig. S3C and S3F). As macrophages also express MPO, we stained for the macrophage cell marker CD68 and found significantly more $CD68^+$ cells adjacent to PanIN in AB-680-treated mice compared to vehicle-treated mice ($P < 0.001$; **Fig. 2E** and **F**). Additionally, in our scRNA-seq data, we noticed increased expression of *CD68* in M2-like macrophages and cDC1 cells (Supplementary Fig. S4A) that play a critical role in initiating and regulating adaptive immune responses. M1 macrophages

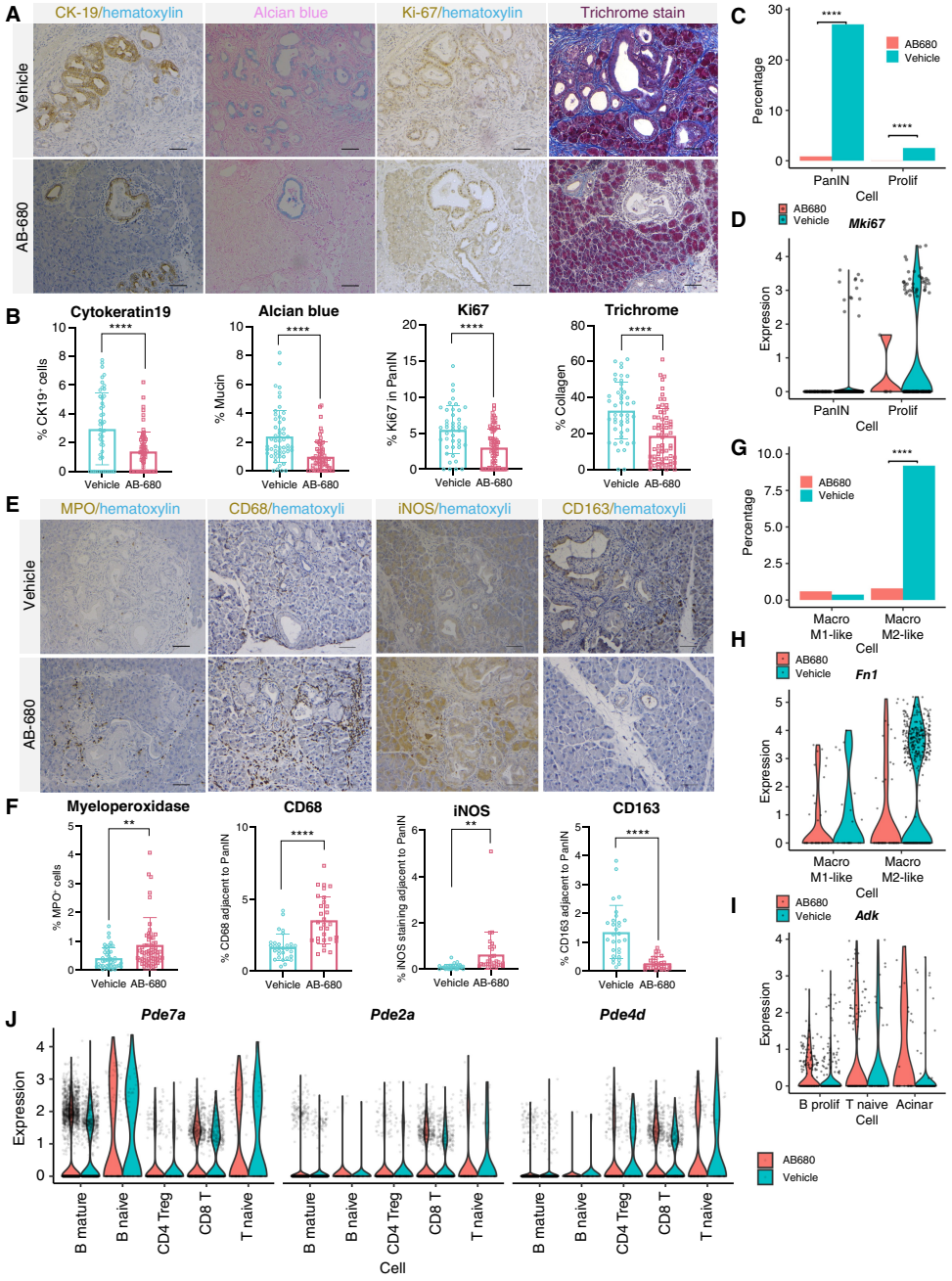

Figure 2.

Oral gavage delivery of a CD73 small molecule inhibitor restrains fibrosis, proliferation, and PanIN progression in *KC* mice. **A,** IHC staining 20× images of CK-19, alcian blue staining, Ki-67, and trichrome staining in pancreas tissue from vehicle control and AB-680 treated mice. **B,** AB-680 treatment significantly decreases CK-19 staining (****, $P < 0.0001$). AB-680 treatment significantly decreases mucin staining (****, $P < 0.0001$). AB-680 treatment significantly decreases Ki-67 staining in PanIN (****, $P < 0.0001$). AB-680 treatment significantly decreases collagen deposition (****, $P < 0.0001$). All quantification was performed in ImageJ, $n = 8$ vehicle control, $n = 11$ AB-680 and six fields per mouse were analyzed. **C,** The proportions of PanIN and proliferative cell populations are significantly lower in AB-680-treated mice. **D,** *Mki67* gene expression levels are lower in PanIN and proliferative cell populations in AB-680 treated mice. **E,** IHC 20× images of Myeloperoxidase (MPO), CD68, iNOS, and CD163 staining in vehicle control and AB-680 mice. **F,** AB-680 significantly increases MPO staining (**, $P = 0.0021$). Quantification was performed in ImageJ, $n = 8$ vehicle control, $n = 11$ AB-680 and six fields per mouse were analyzed. AB-680 significantly increases CD68 staining adjacent to PanIN (****, $P < 0.0001$). AB-680 significantly increases iNOS staining adjacent to PanIN (**, $P =$). AB-680 significantly decreases CD163 staining adjacent to PanIN (****, $P < 0.0001$). Quantification was performed in ImageJ, and $n = 3$ vehicle control, $n = 3$ AB-680, and 10 fields per mouse were analyzed. Statistical analysis was performed using either a Student's *t* test or one-way ANOVA when appropriate in Prism GraphPad software. Scale bars, 50 μm. **G,** The proportion of M2-like macrophage population is significantly lower in AB-680-treated mice. **H,** *Fn1* gene expression level is lower in the M2-like macrophage population in AB-680-treated mice. **I,** *Adk* gene expression levels are higher in proliferative B-cell, naïve T-cell, and acinar cell populations in AB-680-treated mice. **J,** In some immune cell populations, *Pde7a*, *Pde2a*, and *Pde4d* gene expression levels are decreased in AB-680 mice.

elevate CD68, but to confirm our finding, we stained for a more specific M1 macrophage marker, iNOS, and identified significantly more iNOS$^+$ cells adjacent to PanIN in the AB-680-treated mice ($P < 0.01$; **Fig. 2E** and **F**). We then stained for an M2 cell marker, CD163, and found significantly more CD163$^+$ cells adjacent to PanIN in the vehicle control mice compared to the AB-680-treated mice ($P < 0.0001$; **Fig. 2E** and **F**). scRNA-seq data confirmed the significant lower proportion of M2-like macrophages ($P < 0.0001$) and downregulated *Fn1* expression in AB-680-treated mice (**Fig. 2G** and **H**), and *Ifngr1* was elevated in M2-like macrophages and cDC1 in AB-680 treated compared to vehicle-treated mice (Supplementary Fig. S4B). From these data, we conclude significantly more M2 polarized macrophages are present in the vehicle group than in the AB-680-treated group.

CD73 inhibition induces changes in the regulation of intracellular and extracellular adenosine levels

To determine adenosine concentrations *in vivo*, we performed HPLC analysis on the pancreata and serum from *KC* AB-680-treated and vehicle control-treated mice. We previously published AB-680 treatment results in a significant reduction in intratumoral adenosine levels in tumors; however, in this experiment, there was no difference in adenosine concentrations in the pancreas tissue or serum (Supplementary Fig. S5A) between groups. There was also no difference in AMP or inosine levels in either group in the pancreas tissue or serum (Supplementary Fig. S5A and S5B). These data were unexpected, as we hypothesized the CD73 inhibitor AB-680 would decrease the adenosine levels in the AB-680-treated mice. Therefore, we stained for CD73 to examine which cells express CD73 (Supplementary Fig. S5C). We found no significant difference in CD73$^+$ staining per field between groups (Supplementary Fig. S5D); however, we quantified a slight increase in % CD73$^+$ staining per field (Supplementary Fig. S5D). Our scRNA-seq data analysis showed decreased levels of *Slc28a2* (also known as CNT2) in the AB-680-treated group compared to the vehicle, particularly in naive T cells (Supplementary Fig. S5E). This gene encodes a nucleoside transporter involved in the uptake of nucleosides, including adenosine, into cells (31). In addition, in the proliferative B cells, naive T cells, and acinar cells of the AB-680-treated group, there are increased levels of the *Adk* gene encoding for adenosine kinase, which phosphorylates adenosine to AMP (**Fig. 2I**). So, based on our scRNA-seq data, we postulate that the regulation of the intracellular levels of adenosine in these cells has increased in response to AB-680 treatment. Moreover, gene expression of members of phosphodiesterase (PDE) enzyme family (*Pde7a*, *Pde2a*, and *Pde4d*), which are involved in the degradation of cyclic adenosine monophosphate (cAMP) and cyclic guanosine monophosphate (cGMP) have been decreased in some immune cells in the pancreas in response to AB-680 treatment (**Fig. 2J**) indicating complex responses by immune cells in response to AB-680 treatment.

CD73 inhibition results in increased clonotypes and TCR rearrangement

We analyzed the immune repertoire profiles for TCRs to examine the relative abundance and clonal expansion of TCR clonotypes in the AB-680-treated group compared to the vehicle control. We first reclustered scRNA-seq data of T cells to get T-cell subpopulations. We identified a Ccl5$^+$CD8$^+$ T-cell cluster and a gamma-delta T (Tgd) cell cluster not found in the initial clustering (**Fig. 3A**). Our analysis showed that the AB-680-treated group had a higher number of unique TCR clonotypes than the vehicle control group (1389 and 1021 clonotypes, respectively; **Fig. 3B**). We grouped the clonotypes based on their clonal sizes. Unexpanded clonotypes were labeled "Single". Expanded clonotypes with clonal size up to five were labeled "Small"; those with clonal size up to 20 were labeled "Medium," and those with clonal size more than 20 were labeled "Large." The proportion of expanded clonotypes increased in the AB-680-treated group, especially the clonotypes of small and medium size (**Fig. 3C**). After integrating TCR clonotypes with scRNA-seq data, we found that the expanded TCR clonotypes appear in all T-cell subpopulations, suggesting increased clonal expansion in both CD4$^+$ T cells and CD8$^+$ T cells in the AB-680-treated group (**Fig. 3D**). Next, we compared the TCR clonotypes between the two experimental groups and identified some common clonotypes (green points). In particular, the most highly expanded common clonotype had a higher proportion in the AB-680-treated group (**Fig. 3E**). Further examination showed the clonally expanded T cells in all T-cell subpopulations (**Fig. 3F**). The expanded clonotypes in naive T cells may suggest the existence of some memory T cells in this cluster due to their phenotypic similarity. We also found increased clonotype overlap between naive T-cell cluster and CD4$^+$ Th, CD4$^+$ Treg, or CD8$^+$ T-cell clusters in the AB-680-treated group (**Fig. 3G**). The expansion of TCR clones following AB-680 treatment, as opposed to the vehicle control, may stem from various factors. One potential explanation is that AB-680 treatment confers a selective advantage to specific TCR clones in particular cells, possibly those that recognize and target cancer cells or respond to the treatment's effects on the immune system (32).

CD73 inhibition enhances BCR rearrangement and clonal expansion

We analyzed the immune repertoire profiles for BCRs to explore the relative abundance and clonal expansion of BCR clonotypes in the AB-680-treated group compared to the vehicle control. Reclustering of B and plasma cells revealed four plasma cell subpopulations, three of which only appeared in the vehicle control (**Fig. 4A**). Our analysis revealed a significant increase in the total number of unique BCR clonotypes in the AB-680-treated group compared to vehicle control (1878 and 1060 clonotypes, respectively; **Fig. 4B**). Based on clone sizes, BCR clonotypes were

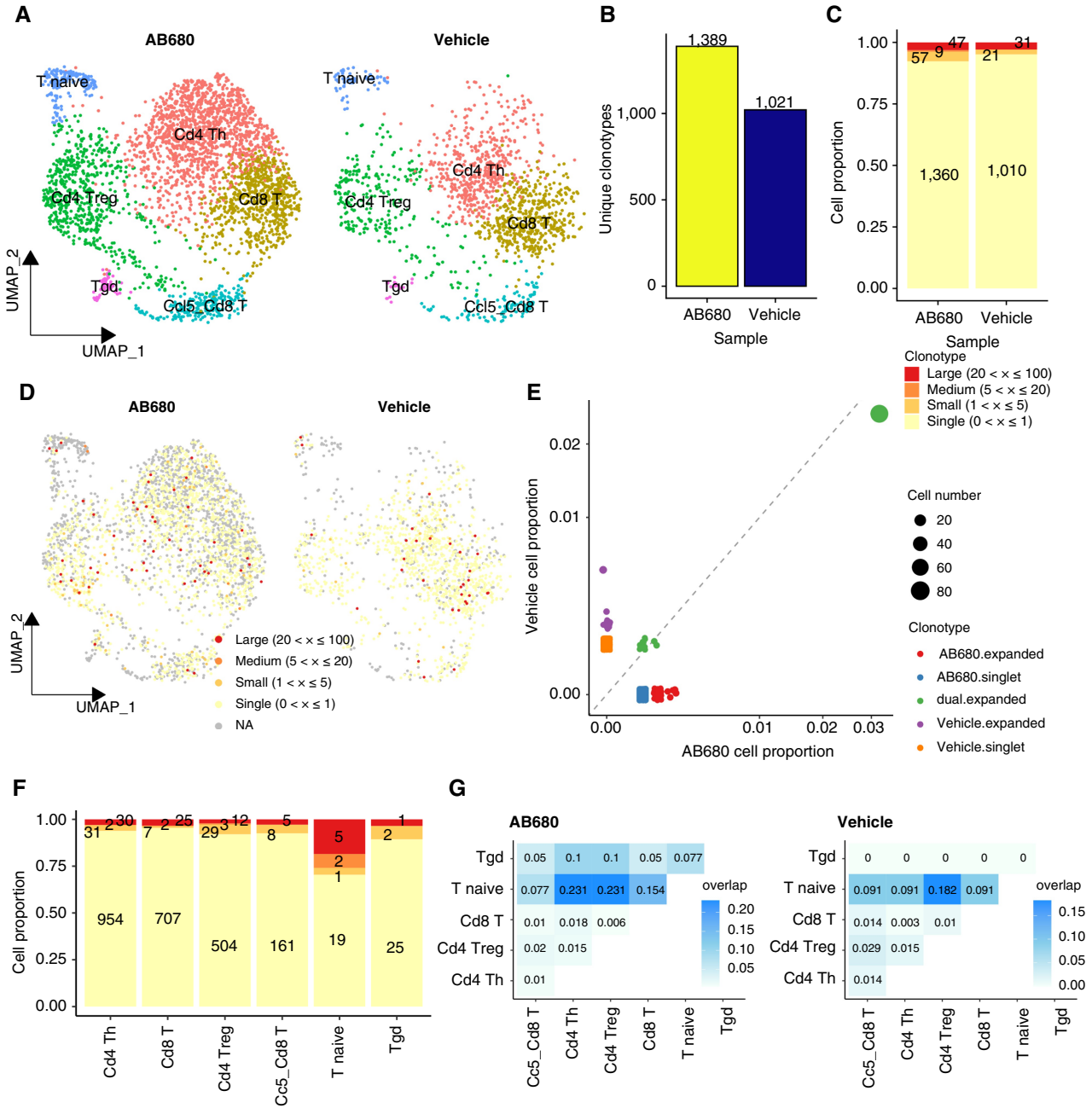

Figure 3.

AB-680 treatment increases TCR clonal expansion in pancreas tissue-infiltrating T cells. **A,** UMAP visualization displays the T-cell subpopulations in AB-680 treated and vehicle control groups. **B,** The number of unique clonotypes in two experimental conditions. **C,** In two conditions, the relative proportion of cells with TCR clonotypes of different clone sizes. **D,** UMAP visualization displaying the TCR clone size of T cells in two conditions. T cells without captured TCR in single-cell TCR sequencing are shown in grey. **E,** Comparison of the proportion of TCR clonotypes between two conditions, including expanded common TCR clonotypes in two conditions (green), expanded unique TCR clonotypes in each condition (red and purple), and unexpanded TCR clonotypes in each condition (blue and orange). **F,** The relative proportion of cells with TCR clonotypes of different clone sizes in T-cell subpopulations. **G,** Clonal overlap of TCR clonotypes within T-cell subpopulations in two conditions, measured by the overlap coefficient.

grouped using the same criteria as TCR clonotypes. Compared to TCRs, there were more clonally expanded BCR clonotypes. The proportion of expanded clonotypes was higher in the AB-680-treated group, especially the clonotypes of medium size (**Fig. 4C**). Comparing the BCR clonal expansion on UMAP showed that mature B cells were most highly clonally expanded in the AB-680-treated group. In contrast, three unique plasma cell clusters were most highly clonally expanded in the vehicle control (**Fig. 4D**). This revealed a significant expansion of large BCR clonotypes in

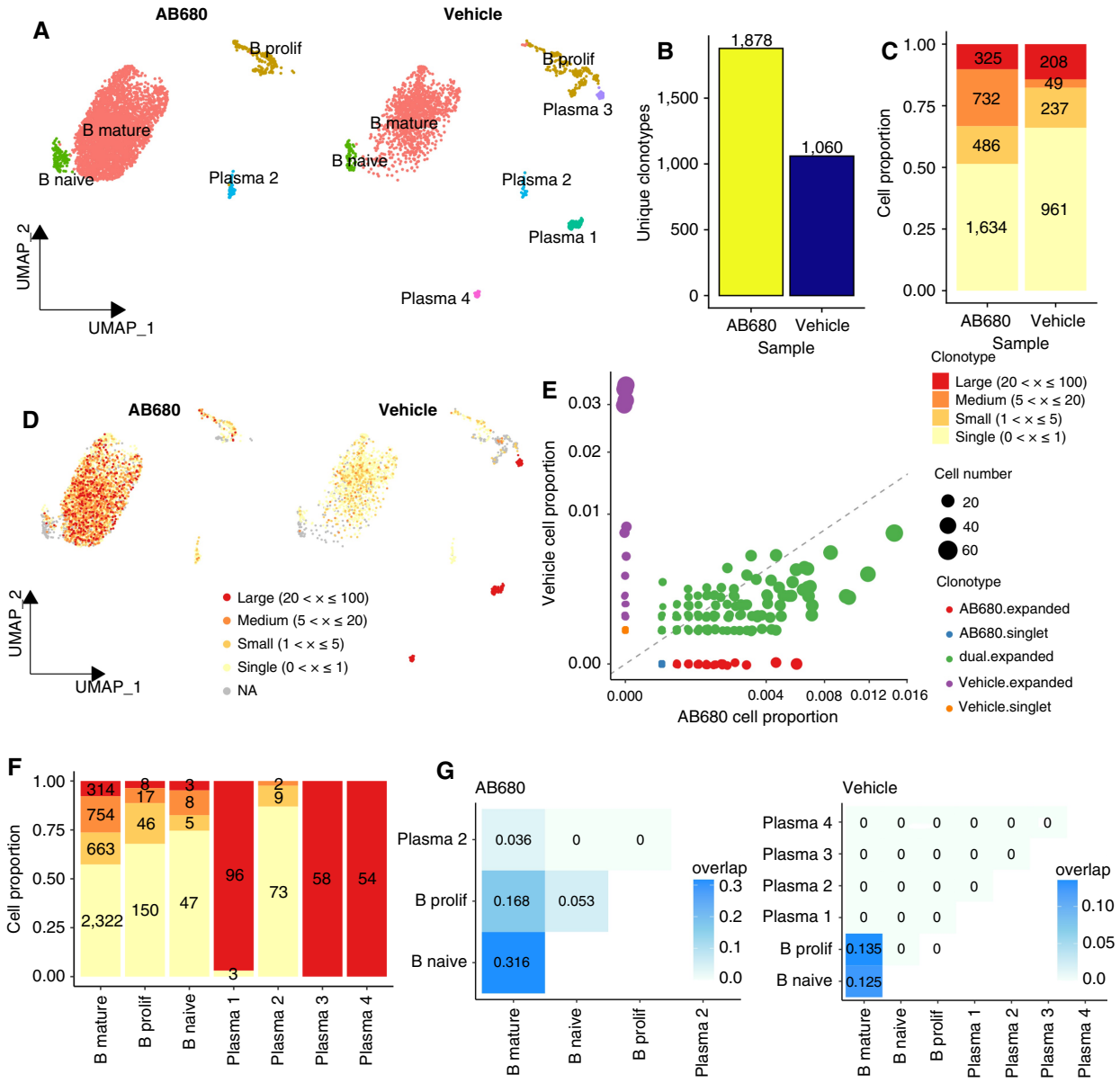

Figure 4.

AB-680 treatment increases BCR clonal expansion in pancreas tissue-infiltrating B cells. **A,** UMAP visualization displays the B-cell subpopulations in AB-680-treated and vehicle control groups. **B,** In two conditions, the relative proportion of cells with BCR clonotypes of different clone sizes. **C,** In two conditions, the relative proportion of cells with BCR clonotypes of different clone sizes. **D,** UMAP visualization displaying the BCR clone size of B cells in two conditions. B cells without captured BCR in single-cell BCR sequencing are shown in gray. **E,** Comparison of the proportion of BCR clonotypes between two conditions, including expanded common BCR clonotypes in two conditions (green), expanded unique BCR clonotypes in each condition (red and purple), and unexpanded BCR clonotypes in each condition (blue and orange). **F,** The relative proportion of cells with BCR clonotypes of different clone sizes in B-cell subpopulations. **G,** Clonal overlap of BCR clonotypes within B-cell subpopulations in two conditions, measured by the overlap coefficient.

mature B cells in the AB-680-treated group compared to the vehicle control. Two experimental groups shared many expanded clonotypes (green points); most of these common clonotypes had a higher proportion in the AB-680-treated group (**Fig. 4E**). Further examination of BCR clonotypes in B-cell subpopulations revealed the highest clonal expansion in vehicle control-specific plasma cell clusters, which is consistent with the UMAP plots (**Fig. 4F**). In addition, the mature B-cell cluster showed higher clonal expansion than proliferative B-cell and naive B-cell clusters. We also found increased clonotype overlap between the naive B-cell cluster and the mature B-cell or the proliferative B-cell clusters in the AB-680-treated group. This suggests enhanced B-cell activation and proliferation in response to AB-680 treatment (**Fig. 4G**).

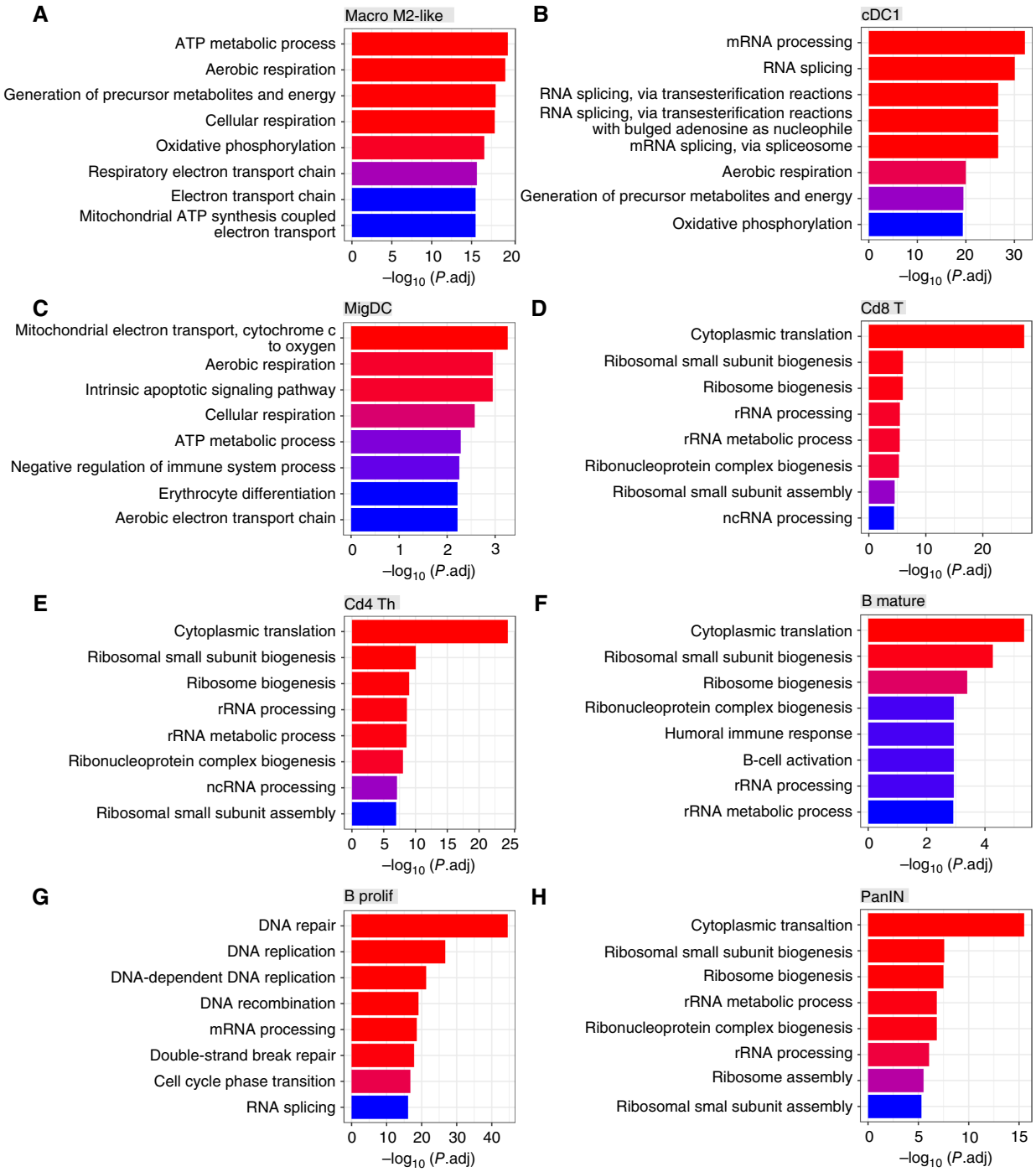

Figure 5.

Blocking CD73 alters distinct biological processes in the immune microenvironment. Gene ontology enrichment analysis reveals top-upregulated biological processes between AB-680-treated mice and vehicle-treated mice in the following cell populations: (**A**) M2-like macrophage, (**B**) cDC1, (**C**) MigDC, (**D**) $CD8^+$ T cell, (**E**) $CD4^+$ helper T cell, (**F**) mature B cell, (**G**) proliferative B cell, and (**H**) PanIN cell.

Blocking CD73 alters distinct biological processes in the immune microenvironment

To gain further insight into the effect of CD73 inhibition on pancreatic biological processes, we performed gene ontological enrichment analysis using the scRNA-seq data. The most common upregulated pathways in multiple immune cell populations were related to cytoplasmic translation and RNA splicing. In the M2-like

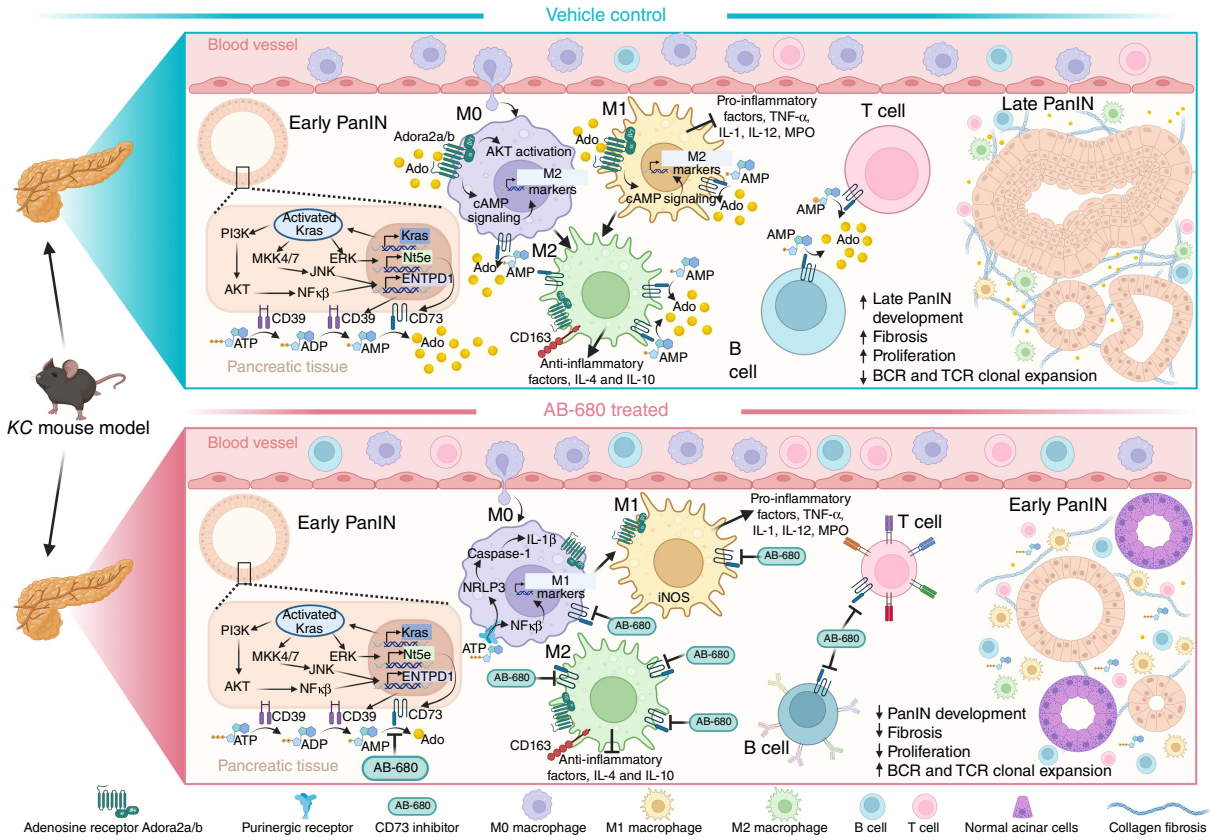

Figure 6.

CD73 inhibition changes the PanIN microenvironment and immune infiltration. Treatment with CD73 inhibitor AB-680 remodels the PanIN microenvironment, increasing M1 macrophages, CD4 and CD8 T-cell infiltration, and TCR clonal expansion. These changes in the immune microenvironment inhibit PanIN development and decrease pancreatic fibrosis. (Credited with BioRender.com.)

macrophages, the top-upregulated biological processes were some energy metabolism-related pathways, such as ATP metabolic process, aerobic respiration, generation of precursor metabolites and energy, and oxidative phosphorylation (**Fig. 5A**). In the cDC1s, the top upregulated biological processes were RNA processing and energy metabolism-related pathways, such as mRNA processing, RNA splicing, aerobic respiration, and oxidative phosphorylation (**Fig. 5B**). In MigDCs, the top upregulated biological processes were energy metabolism-related pathways, such as mitochondrial electron transport, intrinsic apoptotic signaling pathway, cellular respiration, and ATP metabolic process. (**Fig. 5C**). The top upregulated biological processes in the $CD8^+$ T cells were protein translation-related pathways, such as cytoplasmic translation, ribosome biogenesis, rRNA processing, and ribonucleoprotein complex biogenesis (**Fig. 5D**). The top-upregulated biological processes in the $CD4^+$ helper T cells were RNA processing and protein translation-related pathways, such as cytoplasmic translation, ribosome biogenesis, rRNA processing, and ncRNA processing (**Fig. 5E**). The top-upregulated biological processes in the mature B cells were protein translation and immune response–related pathways, such as cytoplasmic translation, ribosome biogenesis, humoral immune response, and B-cell activation (**Fig. 5F**). The top-upregulated biological processes in the proliferative B cells were cell proliferation–related pathways, such as DNA repair, DNA replication, DNA recombination, mRNA processing, and cell cycle phase transition (**Fig. 5G**). In the PanIN cells, the top-upregulated biological processes were protein translation–related pathways, such as cytoplasmic translation, ribosome biogenesis, rRNA processing, and ribosome assembly (**Fig. 5H**).

Discussion

Previous studies incorporating analysis of human PDAC samples through TCGA revealed patients with high CD73 expression have significantly lower overall survival (4). In this study, we wanted to expand upon our previous studies showing that CD73 inhibition with AB-680 reduces tumor growth and volume in KPC subcutaneous tumor models (4, 33). It has been previously demonstrated

that CD73-generated adenosine increases infiltration and polarization of M2 macrophages and MDSCs in KPC subcutaneous tumors (34). However, AB-680 has not been previously studied in the context of cancer prevention. These experiments were conducted in the context of metaplasia and neoplasia. We and others have shown CD73 is expressed in Kras mutant PanIN (4, 35), and in these studies, we found new insight into the relationship between K-Ras signaling in early PanIN and elevated CD73 expression. Our immune profiling provided new insight that CD73 promotes M2 macrophage polarization, fibrosis, and PanIN progression and is an early immune checkpoint that inhibits not only the infiltration of CD4 and CD8 T cells but also reduces TCR clonality in the neoplastic microenvironment (**Fig. 6**).

Our findings are timely as the proinflammatory activities of classically activated macrophages are inhibited by adenosine. When classically activated macrophages interact with adenosine, cytokine, chemokine, and nitric oxide (NO), production is inhibited, which produces anti-inflammatory, or in this context, immune suppressive effects and promotes the growth of PanIN (36). Through the $A_{2B}R$ on macrophages, adenosine can also stimulate the alternatively activated macrophage phenotype induced by IL4 and IL13 (36). Notably, macrophage *Adora2a* and *Adora2b* expression is induced by TLR agonists, allowing macrophages to bind to extracellular adenosine in the tumor microenvironment (36).

ScRNA-seq, TCR, and BCR sequencing analysis also informed us of critical changes in T and B cells in the PanIN microenvironment in the presence of a CD73 inhibitor (**Fig. 6**). Expansion of the TCR and BCR repertoires is important in the adaptive response and suggests CD73 inhibitors can be considered combined with vaccines or other checkpoint inhibitors for immunoprevention. Additionally, CD73 inhibitors should be considered in combination with ablation therapies, including radiofrequency ablation or stereotactic ablative radiotherapy, to enhance the local and abscopal antitumor responses that have been shown to occur in preclinical and clinical studies (33).

AB-680 (quemliclustat) is currently being tested in a phase 1 clinical trial for the treatment of PDAC (NCT04104672), a phase 1/2 clinical trial for the treatment of PDAC (NCT05688215), a phase 2 clinical trial for the treatment of oligometastatic prostate cancer (NCT05915442), a phase 1b/2 clinical trial for the treatment of metastatic colorectal cancer (NCT04660812), and a phase 1b/2 clinical trial for treatment of metastatic castrate-resistant prostate cancer (NCT04381832). However, quemliclustat is not currently being tested in clinical trials for use in the prevention of solid tumors, including pancreatic cancer. Our results indicate quemliclustat treatment in high-risk cohorts or patients with identified PanIN will reduce M2 macrophage polarization and enhance CD4 and CD8 T-cell response to reduce the progression of neoplastic lesions. While promising, more experiments are needed to confirm if inhibition of CD73 in combination with other chemotherapeutic or immunopreventative agents will stop the progression to PDAC. Additionally, future preclinical and clinical studies on mechanisms of therapeutic resistance to CD73 inhibitors should be considered to improve long-term outcomes for patients.

Authors' Disclosures

L.A. Vornik reports other support from MD Anderson Cancer Center during the conduct of the study. M.I. Savage reports other support from NCI during the conduct of the study. P.H. Brown reports other support from GeneTex outside the submitted work. Z. Zhao reports grants from National Institutes of Health and Cancer Prevention and Research Institute of Texas during the conduct of the study. F. McAllister reports personal fees from Neologics Bio outside the submitted work. J.M. Bailey-Lundberg reports grants from National Cancer Institute and other support from National Cancer Institute during the conduct of the study. No disclosures were reported by the other authors.

Authors' Contributions

L.N. Strickland: Data curation, formal analysis, writing–original draft. **W. Liu:** Data curation, formal analysis, writing–review and editing. **U. Hussein:** Data curation, formal analysis, writing–review and editing. **N. Mardik:** Data curation, formal analysis. **X. Chen:** Resources, data curation. **T. Mills:** Data curation. **L.A. Vornik:** Project administration. **M.I. Savage:** Project administration. **S. Sei:** Project administration, writing–review and editing. **J. Clifford:** Project administration. **H.K. Eltzschig:** Resources. **P.H. Brown:** Funding acquisition, project administration. **Z. Zhao:** Data curation. **F. McAllister:** Funding acquisition. **J.M. Bailey-Lundberg:** Conceptualization, resources, formal analysis, supervision, funding acquisition, writing–original draft, project administration.

Acknowledgments

F. McAllister received support from NCI R37 (CA237384), and the Cancer Prevention and Research Institute of Texas (RP200173). J.M. Bailey-Lundberg, F. McAllister, and P.H. Brown received funding from the National Cancer Institute (NCI) Division of Cancer Prevention PREVENT Program Contract No. 75N91019D00021-P00001-759102000002-1 "Preclinical Drug Development Program: Preclinical Efficacy and Intermediate Biomarkers." J.M. Bailey-Lundberg received funding from NCI R21 (CA249924-02) and NCI R01 (CA277161-01A1). Z. Zhou received funding from NCI R01CA27651. H.K. Eltzschig received support from NIH grants R01HL154720, R01DK122796, and R01HL133900. W. Liu is a CPRIT Predoctoral Fellow in the Biomedical Informatics, Genomics, and Translational Cancer Research Training Program (BIG-TCR) funded by the Cancer Prevention & Research Institute of Texas (CPRIT RP210045). We thank lab members of the Bioinformatics Systems Medicine Laboratory (BSML) for their valuable help. Z. Zhao and The UTHealth Cancer Genomics Core generated the sequencing data and are funded by CPRIT (RP180734).

Note

Supplementary data for this article are available at Cancer Prevention Research Online (http://cancerprevres.aacrjournals.org/).

Received April 23, 2024; revised June 25, 2024; accepted August 1, 2024; published first August 3, 2024.

References

1. Carpenter ES, Elhossiny AM, Kadiyala P, Li J, McGue J, Griffith BD, et al. Analysis of donor pancreata defines the transcriptomic signature and microenvironment of early neoplastic lesions. Cancer Discov 2023;13:1324–45.
2. Braxton AM, Kiemen AL, Grahn MP, Forjaz A, Parksong J, Mahesh Babu J, et al. 3D genomic mapping reveals multifocality of human pancreatic precancers. Nature 2024;629:679–87.
3. Zhao J, Soto LMS, Wang H, Katz MH, Prakash LR, Kim M, et al. Overexpression of CD73 in pancreatic ductal adenocarcinoma is associated with immunosuppressive tumor microenvironment and poor survival. Pancreatology 2021;21:942–9.
4. Faraoni EY, Singh K, Chandra V, Le Roux O, Dai Y, Sahin I, et al. CD73-dependent adenosine signaling through Adora2b drives immunosuppression in ductal pancreatic cancer. Cancer Res 2023;83:1111–27.
5. Morrison AH, Byrne KT, Vonderheide RH. Immunotherapy and prevention of pancreatic cancer. Trends Cancer 2018;4:418–28.
6. Clark CE, Hingorani SR, Mick R, Combs C, Tuveson DA, Vonderheide RH. Dynamics of the immune reaction to pancreatic cancer from inception to invasion. Cancer Res 2007;67:9518–27.
7. Burnstock G. Pathophysiology and therapeutic potential of purinergic signaling. Pharmacol Rev 2006;58:58–86.
8. Eltzschig HK, Sitkovsky MV, Robson SC. Purinergic signaling during inflammation. N Engl J Med 2012;367:2322–33.
9. Mayerle J, Sendler M, Hegyi E, Beyer G, Lerch MM, Sahin-Tóth M. Genetics, cell biology, and pathophysiology of pancreatitis. Gastroenterology 2019;156:1951–68.e1.
10. Strickland LN, Faraoni EY, Ruan W, Yuan X, Eltzschig HK, Bailey-Lundberg JM. The resurgence of the Adora2b receptor as an immunotherapeutic target in pancreatic cancer. Front Immunol 2023;14:1163585.
11. Cendrowicz E, Sas Z, Bremer E, Rygiel TP. The role of macrophages in cancer development and therapy. Cancers (Basel) 2021;13:1946.
12. Liou G-Y, Bastea L, Fleming A, Döppler H, Edenfield BH, Dawson DW, et al. The presence of interleukin-13 at pancreatic ADM/PanIN lesions alters macrophage populations and mediates pancreatic tumorigenesis. Cell Rep 2017;19:1322–33.
13. Poh AR, Ernst M. Tumor-associated macrophages in pancreatic ductal adenocarcinoma: therapeutic opportunities and clinical challenges. Cancers (Basel) 2021;13:2860.
14. Pothuri VS, Hogg GD, Conant L, Borcherding N, James CA, Mudd J, et al. Intratumoral T-cell receptor repertoire composition predicts overall survival in patients with pancreatic ductal adenocarcinoma. Oncoimmunology 2024;13:2320411.
15. O'Brien BJ, Faraoni EY, Strickland LN, Ma Z, Mota V, Mota S, et al. CD73-generated extracellular adenosine promotes resolution of neutrophil-mediated tissue injury and restrains metaplasia in pancreatitis. FASEB J 2023;37:e22684.
16. Fleming SJ, Chaffin MD, Arduini A, Akkad A-D, Banks E, Marioni JC, et al. Unsupervised removal of systematic background noise from droplet-based single-cell experiments using CellBender. Nat Methods 2023;20:1323–35.
17. Butler A, Hoffman P, Smibert P, Papalexi E, Satija R. Integrating single-cell transcriptomic data across different conditions, technologies, and species. Nat Biotechnol 2018;36:411–20.
18. Germain P-L, Lun A, Garcia Meixide C, Macnair W, Robinson MD. Doublet identification in single-cell sequencing data using scDblFinder. F1000Res 2021;10:979.
19. Borcherding N, Bormann NL, Kraus G. scRepertoire: an R-based toolkit for single-cell immune receptor analysis. F1000Res 2020;9:47.
20. Wu T, Hu E, Xu S, Chen M, Guo P, Dai Z, et al. clusterProfiler 4.0: a universal enrichment tool for interpreting omics data. Innovation (Camb) 2021;2:100141.
21. Hingorani SR, Petricoin EF, Maitra A, Rajapakse V, King C, Jacobetz MA, et al. Preinvasive and invasive ductal pancreatic cancer and its early detection in the mouse. Cancer Cell 2003;4:437–50.
22. Hruban RH, Adsay NV, Albores-Saavedra J, Compton C, Garrett ES, Goodman SN, et al. Pancreatic intraepithelial neoplasia: a new nomenclature and classification system for pancreatic duct lesions. Am J Surg Pathol 2001;25:579–86.
23. Basturk O, Hong S-M, Wood LD, Adsay NV, Albores-Saavedra J, Biankin AV, et al. A revised classification system and recommendations from the Baltimore Consensus Meeting for neoplastic precursor lesions in the pancreas. Am J Surg Pathol 2015;39:1730–41.
24. Zhao J, Guo C, Xiong F, Yu J, Ge J, Wang H, et al. Single cell RNA-seq reveals the landscape of tumor and infiltrating immune cells in nasopharyngeal carcinoma. Cancer Lett 2020;477:131–43.
25. Kemp SB, Steele NG, Carpenter ES, Donahue KL, Bushnell GG, Morris AH, et al. Pancreatic cancer is marked by complement-high blood monocytes and tumor-associated macrophages. Life Sci Alliance 2021;4:e202000935.
26. Gordon S, Martinez FO. Alternative activation of macrophages: mechanism and functions. Immunity 2010;32:593–604.
27. Cui A, Huang T, Li S, Ma A, Pérez JL, Sander C, et al. Dictionary of immune responses to cytokines at single-cell resolution. Nature 2024;625:377–84.
28. Strnadel J, Choi S, Fujimura K, Wang H, Zhang W, Wyse M, et al. eIF5A-PEAK1 signaling regulates YAP1/TAZ protein expression and pancreatic cancer cell growth. Cancer Res 2017;77:1997–2007.
29. Olaniru OE, Kadolsky U, Kannambath S, Vaikkinen H, Fung K, Dhami P, et al. Single-cell transcriptomic and spatial landscapes of the developing human pancreas. Cell Metab 2023;35:184–99.e5.
30. Nywening TM, Belt BA, Cullinan DR, Panni RZ, Han BJ, Sanford DE, et al. Targeting both tumour-associated $CXCR2^+$ neutrophils and $CCR2^+$ macrophages disrupts myeloid recruitment and improves chemotherapeutic responses in pancreatic ductal adenocarcinoma. Gut 2018;67:1112–23.
31. Young JD, Yao SY, Baldwin JM, Cass CE, Baldwin SA. The human concentrative and equilibrative nucleoside transporter families, SLC28 and SLC29. Mol Aspects Med 2013;34:529–47.
32. Dolton G, Rius C, Wall A, Szomolay B, Bianchi V, Galloway SAE, et al. Targeting of multiple tumor-associated antigens by individual T cell receptors during successful cancer immunotherapy. Cell 2023;186:3333–49.e27.
33. Faraoni EY, Strickland LN, O'Brien BJ, Barraza JF, Thosani NC, Wray CJ, et al. Radiofrequency ablation in combination with CD73 inhibitor AB680 reduces tumor growth and enhances anti-tumor immunity in a syngeneic model of pancreatic ductal adenocarcinoma. Front Oncol 2022;12:995027.
34. Jacoberger-Foissac C, Cousineau I, Bareche Y, Allard D, Chrobak P, Allard B, et al. CD73 inhibits cGAS-STING and cooperates with CD39 to promote pancreatic cancer. Cancer Immunol Res 2023;11:56–71.
35. Singh K, Pruski M, Bland R, Younes M, Guha S, Thosani N, et al. Kras mutation rate precisely orchestrates ductal derived pancreatic intraepithelial neoplasia and pancreatic cancer. Lab Invest 2021;101:177–92.
36. Haskó G, Cronstein B. Regulation of inflammation by adenosine. Front Immunol 2013;4:85.